

Environmentally responsive adsorption and assembly behaviors from *N*-alkyl-1,2-ethylenediamines†

Cite this: *Soft Matter*, 2013, 9, 1458

Yi Yang, Jinfeng Dong, Bo Cai, Zan Jiang, Li Cheng and Xuefeng Li*

A series of pH sensitive single-tailed surfactants, *N*-alkyl-1,2-ethylenediamine (C_mN2N , where $m = 8, 10, 12, 14, 16$), were synthesized and characterized. The adsorption and aggregation properties of them were determined by equilibrium surface tension, static and dynamic light scattering (SLS and DLS), rheology, and cryogenic transmission electron microscopy (cryo-TEM) techniques in detail. It was found that both the surface activity and self-assembly behavior of C_mN2N were strongly dependent on the solution pH, owing to the protonation state of amino groups in C_mN2N . When at least one of the amino groups of C_mN2N was protonated the logarithm of the critical micelle concentration (cmc) followed the well-known Klevens equation, *i.e.* cmc decreased linearly with the increase of hydrocarbon chain length. Simultaneously, the surface adsorption area per molecule (A_{min}) was decreased for each C_mN2N when the solution pH varied from acidic to basic conditions. The pH-dependent micelle to vesicle transition was universally observed in the bulk phase of C_mN2N . More interestingly, the rodlike micelles formed in $C_{10}N2N$, $C_{12}N2N$ and $C_{14}N2N$ could transform into vesicles reversibly upon heating or cooling, which indicated the thermal sensitivity of organized assemblies, whereas not in $C_{8}N2N$ and $C_{16}N2N$.

Received 4th October 2012

Accepted 20th November 2012

DOI: 10.1039/c2sm27288a

www.rsc.org/softmatter

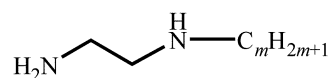
1 Introduction

Environmentally responsive surfactants exhibit adsorption or assembly behaviors controllable by light,^{1,2} magnetic field,^{3,4} redox reaction,⁵ electrolytes,^{6–8} pH^{9–11} and temperature,^{12–14} and have bright prospective applications in designing novel materials, enhancing oil recovery, gene and drug delivery controlled release, DNA regulation, environmental management and clutches for transmission, *etc.*^{15–20} The fabrication of novel surfactants with environmental sensitivity and the realization of a synergic regulation of weak interactions are the most studied, currently. pH responsive surfactants, such as fatty acids,^{21–24} alkylamine oxides^{25–27} and alkylamines,^{28,29} were widely investigated, where the pH-dependent adsorption and self-assembly behaviors were mainly caused by the composition variation between the unprotonated nonionic partners and the protonated ionic ones.

Monoalkyldiamines are structurally similar to alkylamines, and hence are pH responsive. They are readily coordinated with heavy metal ions such as Cu^{2+} or Co^{3+} strongly due to the two amino groups presented in their hydrophilic part,^{30–34} which have important applications in industry as floating chemicals. Compared to the pH sensitivity, the properties of the ligands have rarely been addressed.^{12,13,35,36} Studies are mainly focused

on the metal ion induced vesicle formation,^{30–34} whereas the effect of the species distribution caused by the ionization equilibria has often been neglected in vesiculation. It has been demonstrated that micelles and vesicles can be formed in dodecyldiamine aqueous solutions at acidic and basic conditions, respectively, regardless of the spacer length between the two amino groups.^{12,13} Furthermore, thermally reversible micelle to vesicle transitions were universally observed in those systems. From the point of view of molecular structures, monoalkyldiamines are single-tailed surfactants containing two headgroups. Worthy of note, the number of headgroups in such single-tailed surfactants were proved to be critical in determining their physicochemical properties, such as critical micelle concentration (cmc), aggregation number, micellar shape, *etc.*³⁷

Beyond the influence of the spacer length between the two amino groups on the aggregation behavior in dodecyldiamine systems,^{12,13} the motivation of the present work is to verify the effect of the hydrophobic length on the pH-dependent adsorption and self-assembly behaviors of *N*-monoalkyl-1,2-ethylenediamines (C_mN2N , $m = 8, 10, 12, 14, 16$; Scheme 1), and



C_mN2N , $m = 8, 10, 12, 14, 16$

Scheme 1 The molecular structures of *N*-monoalkyl-1,2-ethylenediamines C_mN2N .

College of Chemistry and Molecules Sciences, Wuhan University, Wuhan, 430072, PR China. E-mail: lixf_wuhu@163.com

† Electronic supplementary information (ESI) available. See DOI: 10.1039/c2sm27288a

establish the molecular structure–property relationship. Though, the aggregation behaviors of *CmN2N* homologues have been reported previously,³⁵ its pH dependency has not been revealed. Moreover, the surface properties have not been studied yet. Herein, the effects of the hydrophobic chain length, pH, electrolytes and temperature on the surface and bulk properties of *CmN2N* were studied in detail by employing equilibrium surface tension, static and dynamic light scattering (SLS and DLS), rheology, and cryogenic transmission electron microscopy (cryo-TEM) measurements. This is of fundamental importance in understanding surfactant properties at the molecular level, and is valuable for their further applications in enhancing oil recovery, demulsification, nano-material synthesis, controlled drug release, *etc.*^{15–20}

2 Materials and methods

2.1 Materials

1,2-Ethanediamine (98%) and *n*-alkyl bromide ($C_nH_{2n+1}Br$, $n = 8, 10, 12, 14, 16$; 98%) were all obtained from TCI. Dichloromethane, methanol, NaOH, HCl, and KI were analytical grade and purchased from the Chinese Medical Company (Shanghai). All reagents were used as received. *CmN2N* was synthesized directly from 1,2-ethanediamine with *n*-alkyl bromide in the presence of a small amount of KI at 110 °C for 24 h (ref. 35) and purified over silica gel using dichloromethane–methanol as the eluent. C8N2N: ¹H NMR (300 MHz, CDCl₃) 0.88 (*t*, 3H, CH₃); 1.24 (*s*, 10H, CH₂); 1.48 (*s*, 2H, CH₂); 2.59, 2.68 (*2t*, 4H, NH₂–CH₂–CH₂–NH); 2.81 (*t*, 2H, –CH₂–NH₂). ESI-MS *m/z* expected ([M + H]⁺) 173.2, found 173.2. C10N2N: ¹H NMR (300 MHz, CDCl₃) 0.88 (*t*, 3H, CH₃); 1.24 (*s*, 14H, CH₂); 1.48 (*s*, 2H, CH₂); 2.59, 2.68 (*2t*, 4H, NH₂–CH₂–CH₂–NH); 2.81 (*t*, 2H, –CH₂–NH₂). ESI-MS *m/z* expected ([M + H]⁺) 201.2, found 201.2. C12N2N: ¹H NMR (300 MHz, CDCl₃) 0.88 (*t*, 3H, CH₃); 1.24 (*s*, 18H, CH₂); 1.48 (*s*, 2H, CH₂); 2.59, 2.68 (*2t*, 4H, NH₂–CH₂–CH₂–NH); 2.81 (*t*, 2H, –CH₂–NH₂). ESI-MS *m/z* expected ([M + H]⁺) 229.2, found 229.2. C14N2N: ¹H NMR (300 MHz, CDCl₃) 0.88 (*t*, 3H, CH₃); 1.24 (*s*, 22H, CH₂); 1.47 (*s*, 2H, CH₂); 2.58, 2.67 (*2t*, 4H, NH₂–CH₂–CH₂–NH); 2.80 (*t*, 2H, –CH₂–NH₂). ESI-MS *m/z* expected ([M + H]⁺) 257.3, found 257.3. C16N2N: ¹H NMR (300 MHz, CDCl₃) 0.88 (*t*, 3H, CH₃); 1.24 (*s*, 26H, CH₂); 1.47 (*s*, 2H, CH₂); 2.58, 2.67 (*2t*, 4H, NH₂–CH₂–CH₂–NH); 2.80 (*t*, 2H, –CH₂–NH₂). ESI-MS *m/z* expected ([M + H]⁺) 285.3, found 285.3.

2.2 Sample preparation

Dispersions of *CmN2N* in water (Millipore) were prepared by the direct sonication of the appropriate chemicals in water, and the dispersions were stable and uniformly bluish. It must be noted that C8N2N, C10N2N and C12N2N were prepared at 25 °C, whereas C14N2N and C16N2N were prepared at 40 °C and 50 °C, respectively, due to their low solubility in an aqueous solution at room temperature. Therefore all measurements were performed at the same corresponding temperature for each *CmN2N* without further discussion. Samples with required pH values, which were measured by a Rex model PHSJ-5 digital pH meter (Leici, China) with a temperature sensor using an E-201D

combination pH electrode, were prepared by titrating with hydrochloric acid or sodium hydroxide aqueous solutions directly. All the samples were equilibrated overnight before each measurement.

2.3 pH titration

pH titration was performed on a Rex model PHSJ-5 digital pH meter (Leici, China) with a temperature sensor using an E-201D combination pH electrode. Hydrochloric acid aqueous solution was initially added to 10 mL *CmN2N* aqueous dispersions until pH ~ 2, and was then subsequently titrated with 1 mol L⁻¹ sodium hydroxide aqueous solution. Each titration point was recorded until the potential drift was stable.

2.4 Surface tension measurement

The surface tension of *CmN2N* aqueous solutions was measured by the Du Nouy ring method (Krüss K100, Germany). The adsorption amount was calculated according to the Gibbs adsorption equation:^{10,11}

$$\Gamma_{\max} = -\frac{1}{2.303nRT} \times \frac{d\gamma}{d \log c} \quad (1)$$

where Γ_{\max} is the saturated adsorption amount in $\mu\text{mol m}^{-2}$, γ is the surface tension in mN m^{-1} , R is the gas constant, T is the absolute temperature, and c is the surfactant concentration. $(d\gamma/d \log c)$ is the slope of the γ - $\log c$ curve when the surfactant concentration is below the cmc, and the value of n is dependent on the specific circumstances.³⁸ The minimum average occupied area per molecule (A_{\min}) is obtained from the saturated adsorption using eqn (2):

$$A_{\min} = \frac{1}{N_A \Gamma_{\max}} \times 10^{24} \quad (2)$$

where N_A is the Avogadro constant and A_{\min} is in nm^2 .

2.5 Static and dynamic light scattering

Static and dynamic light scattering (SLS and DLS) measurements were performed on the Zetasizer instrument ZEN3600 (Malvern, UK) with a 173° back scattering angle and He–Ne laser ($\lambda = 633 \text{ nm}$). Samples were filtered with a 0.2 μm filter of mixed cellulose acetate to remove any interfering dust particles. The pH-dependent intensities from SLS experiments were performed after the samples with the required pH were equilibrated overnight. The temperature dependent intensities were measured as the sample was equilibrated for 10 minutes at each 2.5 °C temperature jump. The experimental data were normalized such that the curves overlap, and the pH or temperature of the transitions was more clearly displayed. To obtain the apparent hydrodynamic radius ($R_{h,\text{app}}$), the intensity autocorrelation functions were analyzed using CONTIN.

2.6 Rheological measurements

Rheological measurements were performed on the RS 600 stress-controlled rheometer (TA Instruments, Germany) using the Coette geometries DG 41, which were equipped with a Peltier-based temperature control. A solvent trap was used to

minimize the sample evaporation. The temperature dependent viscosity was measured as the sample was equilibrated for 20 minutes at each temperature jump.

2.7 Cryo-transmission electron microscopy

Samples for cryo-TEM were prepared as follows: 3–5 μL of sample dispersion was deposited on the surface of a TEM copper grid covered by a holey carbon film. After blotting away the excess dispersion to form a thin liquid film, the grid was immediately plunged into liquid ethane. The specimens were maintained at approximately $-173\text{ }^\circ\text{C}$ ($I\text{-N}_2$) and imaged in a transmission electron microscope (JEOL 2010) at an accelerating voltage of 200 kV under low dose conditions.

3 Results and discussion

3.1 Protonation of $CmN2N$ surfactants

One of the most important features of $CmN2N$ is the pH sensitivity due to the presence of two pH sensitive amino groups in the hydrophilic part, which can be protonated in acidic conditions. The surfactant molecules can be divalent cationic (H_2A^{2+}), monovalent cationic (HA^+) and nonionic (A) by varying the solution pH. The pH-dependent ionizable headgroups for each $CmN2N$ were determined by pH titration, and two distinguished $\text{p}K_{\text{a}}$ values were obtained as summarized in Table 1. It was observed that both $\text{p}K_{\text{a}_1}$ and $\text{p}K_{\text{a}_2}$ were decreased slightly with the increase of the hydrophobic chain length m , which is similar to fatty acids³⁹ or N,N' -dialkyl- N,N' -di(ethyl-2-pyrrolidone) ethylenediamine homologues.¹¹ Based on the calculation from the apparent $\text{p}K_{\text{a}}$ values, the species distribution of $CmN2N$ in an aqueous solution was obtained (ESI Fig. S1†), which is essential in understanding the importance of ionic species on the surface and aggregation properties.

3.2 Equilibrium surface tensions

In order to evaluate the surface activity and adsorption behavior of $CmN2N$ in an aqueous solution, the equilibrium surface tension at different pH and concentrations was investigated by employing du Nouy tensiometry. The results of surface tension measurements at pH = 2.0, 7.5 and 11.0 presented in a semi logarithmic representation are shown in Fig. 1a–c, respectively.

Obviously, $CmN2N$ exhibits the classic surface tension–concentration relationship when m varies from 8 to 16 both at pH = 2.0 and 7.5. The clear breakpoint in the $\gamma\text{-log } c$ curve at a certain concentration corresponds to its cmc, indicating the onset of micellization. The absence of a minimum around the

breakpoint confirms the purity of the surfactants. It should be mentioned that $CmN2N$ has a poor solubility in an aqueous solution at pH = 11.0, which inhibits the surface tension measurement by adsorption above the cmc. However, the slope of the $\gamma\text{-log } c$ curves below cmc is essentially constant, indicating that the surface concentration has reached a constant maximum value. In the typical $\gamma\text{-log } c$ plots for the diluted solution of surfactants before micellization, the surface tension decreases normally and matched the well-known Gibbs equation. For surfactant concentrations below but near the cmc, the slope of the curve is essentially constant, indicating that the surface concentration has reached a constant maximum value. In this range the interface is considered to be saturated with surfactant molecules and the continued reduction in the surface tension is mainly due to the increased activity of the surfactant in the bulk phase rather than at the interface.⁴⁰ Though, the theory was recently questioned by Menger *et al.* with new evidence that surfactant molecules are cooperatively adsorbed rather than saturated in this region.^{41,42} However, the consistent understanding about this new theory is not made yet,^{43,44} and hence the Gibbs analysis is employed in this work. The important physicochemical parameters of $CmN2N$ extracted from the $\gamma\text{-log } c$ curves, such as cmc, surface tension at cmc (γ_{cmc}), T_{max} and A_{min} , are summarized in Table 2. For divalent cationic, monovalent cationic and nonionic type surfactants of $CmN2N$ at pH = 2.0, 7.5 and 11, n is taken as 3, 2 and 1, respectively.

The cmc values of surfactant homologues often follow the well-known Klevens empirical eqn (3) where cmc decreases linearly with the increase of the carbon atom number m in the hydrocarbon chain.⁴⁵

$$\log \text{cmc} = A - B \times m \quad (3)$$

where A and B are the empirical constants. Generally, A reflects the nature and numbers of the hydrophilic group, while B represents the contribution of each additional methylene unit on the cmc. Two linear equations, $\log \text{cmc}_{\text{pH}=2.0} = 1.23 - 0.288 \times m$ and $\log \text{cmc}_{\text{pH}=7.5} = 0.057 - 0.252 \times m$, were obtained for $CmN2N$ at pH = 2.0 and 7.5 (Fig. 2), respectively. Clearly, the two values of A are significantly different, which can be attributed to the protonation states of $CmN2N$ as shown in Fig. S1.† Simultaneously, a limited difference is observed for the values of B , suggesting the influence of each additional methylene unit on cmc is similar at both conditions.

Between the empirical equation of $CmN2N$ at pH = 2.0 and that of alkylammonium chloride ($Cm\text{NH}_3\text{Cl}$, $\log \text{cmc} = 1.25 - 0.295 \times m$) at $25\text{ }^\circ\text{C}$,⁴⁶ where all surfactants are fully protonated, no significant difference can be observed except that the cmc of $Cm\text{NH}_3\text{Cl}$ is slightly smaller than that of $CmN2N$ at pH = 2.0 with the same m . This means that the chemical combination of an additional amino group in the hydrophilic headgroup increased the hydrophilicity but decreased the micellization ability of the surfactant, which has also been observed in the bifunctional N-oxides of alkyldiamidamines.^{47,48} Similarly to cmc, when m increases, the values of γ_{cmc} are also decreased at pH = 2.0 and 7.5, following the general rule of surfactants. This

Table 1 $\text{p}K_{\text{a}}$ values of $CmN2N$ ($m = 8, 10, 12, 14, 16$)

Surfactants	c (mol L^{-1})	T ($^\circ\text{C}$)	$\text{p}K_{\text{a}_1}$	$\text{p}K_{\text{a}_2}$
C8N2N	0.1	25	4.35	11.18
C10N2N	0.075	25	4.16	11.05
C12N2N	0.05	25	4.03	10.63
C14N2N	0.025	40	3.76	10.12
C16N2N	0.0125	50	3.63	9.91

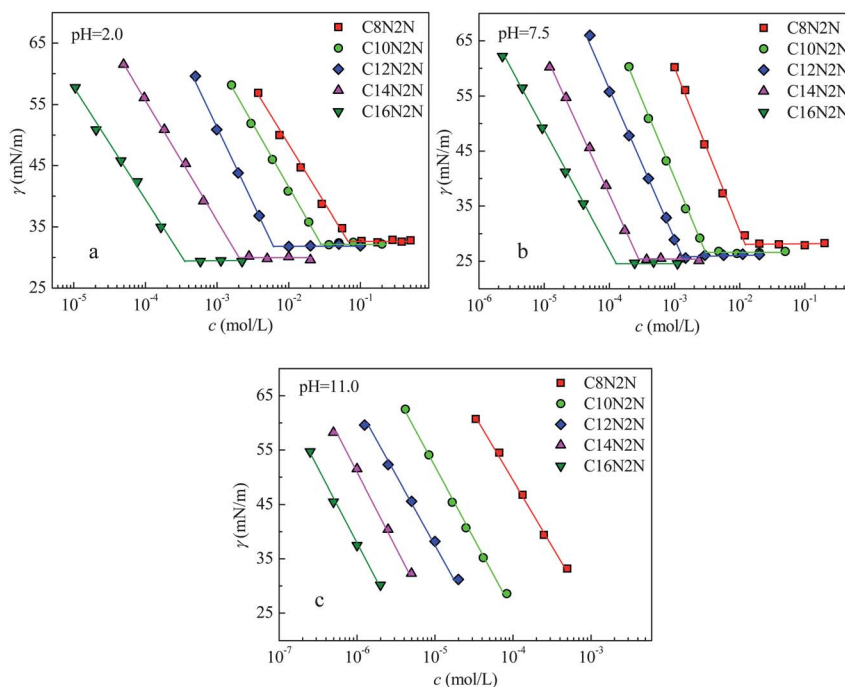


Fig. 1 The γ -log c plots of C_mN_2N in aqueous solutions at pH 2.0 (a), 7.5 (b) and 11.0 (c).

is because surfactants with longer alkyl chains adsorb more strongly at the air-water interface than shorter ones due to the stronger hydrophobic interaction and this results in a lower γ_{cmc} .

The value of n in the Gibbs eqn (1) presents uncertainty in explaining the packing densities of ionic surfactants due to the adsorption of counter ions,^{11,49,50} whereas $n = 1$ can be employed simply in the presence of an additional electrolyte. To avoid

Table 2 Surface properties of C_mN_2N ($m = 8, 10, 12, 14, 16$)

Surfactants	Environmental conditions				γ_{cmc} (mN m ⁻¹)	Γ_{max} ($\mu\text{mol m}^{-2}$)	A_{min} (nm ²)
	T (°C)	pH	[NaCl] (mol L ⁻¹)	cmc (mol L ⁻¹)			
C8N2N	25	2.0	0	0.073	32.7	1.10	1.51
			0.2	0.026	29.5	2.67	0.62
		7.5	0	0.012	27.8	2.55	0.65
			0.05	0.0036	27.1	3.34	0.50
			0	—	—	4.20	0.40
C10N2N	25	2.0	0	0.026	32.3	1.22	1.36
			0.1	0.014	30.3	2.74	0.61
		7.5	0	0.003	26.7	2.51	0.66
			0.02	0.0014	26.1	3.16	0.53
			0	—	—	4.47	0.37
C12N2N	25	2.0	0	0.0058	31.9	1.49	1.12
			0.05	0.0049	29.5	2.51	0.66
		7.5	0	0.0013	26.1	2.44	0.68
			0.01	0.00034	25.5	3.05	0.54
			0	—	—	4.13	0.40
C14N2N	40	2.0	0	0.002	29.9	1.09	1.52
			0.02	0.0013	28.6	2.48	0.67
		7.5	0	0.00028	25.3	2.15	0.77
			0.005	0.000066	24.8	3.45	0.48
			0	—	—	4.37	0.38
C16N2N	50	2.0	0	0.00035	29.5	0.98	1.68
			0.01	0.00032	28.2	2.35	0.71
		7.5	0	0.00012	24.8	1.77	0.94
			0.002	0.000026	24.5	3.63	0.46
			0	—	—	4.38	0.38

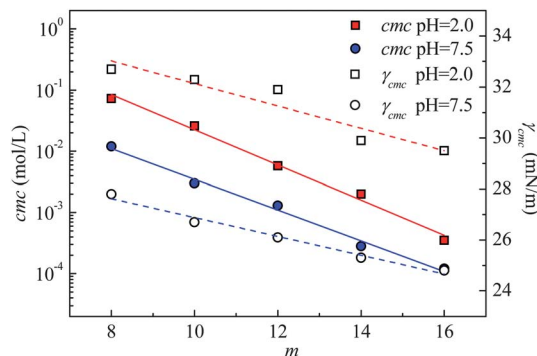


Fig. 2 The cmc and γ_{cmc} of C_mN_{2N} as a function of the number of carbon atoms in the hydrophobic chains.

this, the equilibrium surface tension of ionic type C_mN_{2N} in the presence of NaCl at pH = 2.0 and 7.5 was measured as shown in Fig. 3, and the corresponding surface properties are also summarized in Table 2. It should be mentioned that the concentration of NaCl added was varied for each C_mN_{2N} at different pH values, according to the difference in the cmc. It is observed that all the values of cmc, γ_{cmc} and A_{min} are decreased in the presence of NaCl. This is due to the reduction in the electrostatic repulsion among the hydrophilic headgroups where the binding of counter ions is the major cause.⁵¹ The effects of the ionic strength and temperature on the adsorption for C_mN_{2N} homologues cannot be neglected, as they hinder the creation of the relationship between m and A_{min} . However, the values of A_{min} clarify an important trend for each C_mN_{2N} , that A_{min} is decreased significantly with the increase in pH, which could mostly be attributed to the different effect of the electrostatic repulsion among hydrophilic headgroups.^{11,51} For example, the values of A_{min} are 0.63 ± 0.03 , 0.52 ± 0.02 and $0.39 \pm 0.02 \text{ nm}^2$ at pH = 2.0, 7.5 and 11.0, respectively, for C8N2N to C12N2N at 25 °C.

3.3 Environmental stimuli-responsive aggregation behaviors of C_mN_{2N}

3.3.1 pH INDUCED MICELLE TO VESICLE TRANSITION. According to the cmc values of C_mN_{2N} obtained from the equilibrium surface tension measurements, the concentrations of 0.1, 0.075, 0.05, 0.025 and 0.0125 mol L⁻¹ were employed for C8N2N,

C10N2N, C12N2N, C14N2N and C16N2N, respectively, which guaranteed that the aggregates were formed in the pH region investigated for each C_mN_{2N} . Uniform phenomena were observed by SLS, as shown in Fig. 4a, in which all the solutions were transformed from optically transparent to bluish as the solution was varied from acidic to basic conditions for each C_mN_{2N} . It was noticed that the scattering intensity was increased steeply once the solution pH was above a special value for each C_mN_{2N} , and then remained nearly constant. The obvious difference came from the values of pH where the transitions occurred. Moreover, the values of pH were decreased with the increasing carbon number m , i.e. around 10.0 and 6.0 for C8N2N and C16N2N, respectively.

The SLS results indicated that aggregates with different morphologies were formed by varying the solution pH. In order to clarify the size of those aggregates, DLS measurements were performed for each C_mN_{2N} at five representative pH values. The results of C10N2N are shown in Fig. 4b, and similar results for C8N2N, C12N2N, C14N2N and C16N2N are shown in ESI Fig. S2.† Generally, narrow monomodal size distributions with the apparent hydrodynamic radius $R_{h,\text{app}} \sim 2 \text{ nm}$ were obtained at pH = 2.00 and 8.14, respectively, suggesting the formation of spherical micelles. The size distribution became broad and bimodal at pH = 9.15, which was just located in the scattering light intensity jump region, indicating that larger aggregates were formed. Considering the dramatic increase in scattering light intensity and broad size distribution, the aggregates might possess a cylindrical shape. Finally, monomodal size distributions with $R_{h,\text{app}} \sim 30$ and 70 nm were observed at pH = 9.47 and 10.30, respectively, suggesting the formation of vesicles.

In order to clarify the presence of rodlike/wormlike micelles, typical steady-shear rheology curves of C_mN_{2N} located in the light scattering jump pH region are shown in Fig. 5a. Roughly, they can be divided into three groups. Firstly, the viscosity of C8N2N was as low as water and kept nearly constant regardless of the shear rate. Secondly, the curves of C10N2N, C12N2N and C14N2N underwent the shear thickening transition when the shear rate reached a critical value $\dot{\gamma}_c$. The overall behavior is the same for all three surfactants, and the only difference came from the slight shift of both the characteristic shear rates and viscosity values towards the upper-left from C10N2N to C14N2N. Similar shear thickening transitions were often observed in rodlike micelle formation systems, such as the

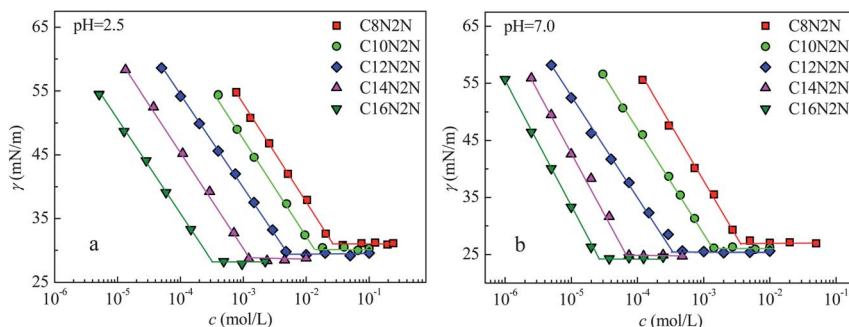


Fig. 3 The γ -log c plots of C_mN_{2N} aqueous solutions in the presence of NaCl at pH 2.0 (a) and 7.5 (b), respectively.

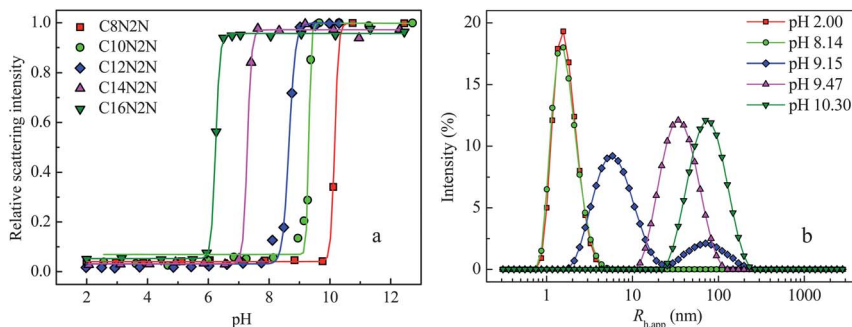


Fig. 4 (a) The scattered light intensity at $\theta = 173^\circ$ as a function of pH of 0.1 mol L^{-1} C8N2N, 0.075 mol L^{-1} C10N2N and 0.05 mol L^{-1} C12N2N at 25°C , 0.025 mol L^{-1} C14N2N at 40°C and $0.0125 \text{ mol L}^{-1}$ C16N2N at 50°C ; (b) pH-dependent apparent hydrodynamic radius $R_{h,app}$ of 0.075 mol L^{-1} C10N2N at 25°C .

cetyltrimethylammonium–sodium salicylate binary system where γ_c was a function of the micellar length.⁵² Specifically, the decrease of γ_c indicates the increase of micellar length. The results suggest that the micellar length was increased from C10N2N to C14N2N. Thirdly, shear thinning behavior was observed in C16N2N, which was often observed in wormlike micelle systems that possessed a longer micellar length,^{5,8,9,14} suggesting that wormlike micelles might be formed in C16N2N. The viscosity results indicated that the micellar length or the micro-structure of micelles located in the special light scattering jump pH region was dependent on the hydrophobic chain length of $CmN2N$.

Moreover, it was noticed that the shear thickening behavior was a function of solution pH. The typical effect of pH on C14N2N is shown in Fig. 5b. It was observed that the viscosity of C14N2N was increased with the decrease of γ_c from pH = 7.26 to 7.50, which indicated micellar growth. At pH = 7.61, a maximum viscosity was observed with the shear thickening behavior weakened. When the solution pH was increased to 7.71 and 7.88, the viscosity decreased with a slight increase of γ_c . A further increase in pH of the solution would result in the disappearance of the shear thickening behavior due to the formation of vesicles. Similar pH-dependent shear thickening behaviors of C10N2N and C12N2N are shown in ESI Fig. S3.† The results indicate that the micellar micro-structure located in the special light scattering jump pH region was strongly dependent on the solution pH.

The light scattering and viscosity results suggested that $CmN2N$ ($m = 10, 12, 14, 16$) possessed a pH-dependent spherical micelle to vesicle transition via a rodlike/wormlike micelle. In order to clarify the aggregates' micro-structural features, the morphologies of aggregates were further studied by employing cryo-TEM measurements. Fig. 6a–d show the micellar micro-structures of $CmN2N$ located in the special light scattering jump pH region. Specifically, C10N2N at pH = 9.15, C12N2N at pH = 8.48, C14N2N at pH = 7.55 and C16N2N at pH = 6.26, respectively. It was observed that rodlike/wormlike micelles were formed.

It was noticed that all samples became turbid at higher pH values for $CmN2N$, and the DLS results of them at higher pH values indicates a similar phenomenon, in which a monomodal size distribution with an $R_{h,app}$ around 100 nm is observed, suggesting vesicle formation. For example, the $R_{h,app}$ of C8N2N at pH 10.75 and of C16N2N at pH 8.28 was 82 and 71 nm (ESI Fig. S2†), respectively. The aggregates' morphologies were further studied by cryo-TEM, and images of C8N2N at pH = 10.11, C10N2N at pH = 10.51, C12N2N at pH = 9.80, C14N2N at pH = 8.83 and C16N2N at pH = 8.28 are shown in Fig. 7. Obviously, vesicles were formed for each $CmN2N$. Thus, it can be concluded that the aggregates of $CmN2N$ amphiphiles experience the pH-responsive micelle to vesicle transition as the pH varies from acidic to basic conditions.

The SLS, DLS, cryo-TEM and viscosity results demonstrated that $CmN2N$ underwent pH-responsive micelle to vesicle

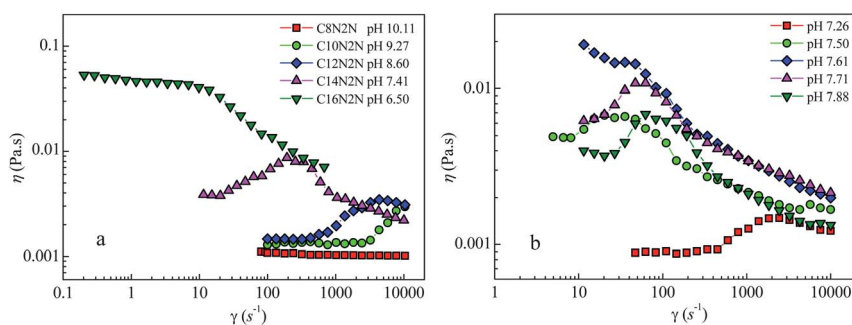


Fig. 5 (a) The steady-shear rheology of 0.1 mol L^{-1} C8N2N at pH 10.11, 0.075 mol L^{-1} C10N2N at pH 9.27 and 0.05 mol L^{-1} C12N2N at pH 8.60 at 25°C , 0.025 mol L^{-1} C14N2N at pH 7.41 at 40°C and $0.0125 \text{ mol L}^{-1}$ C16N2N at pH 6.50 at 50°C as a function of shear rate; (b) the steady-shear rheology of 0.025 mol L^{-1} C14N2N at 40°C as a function of pH.

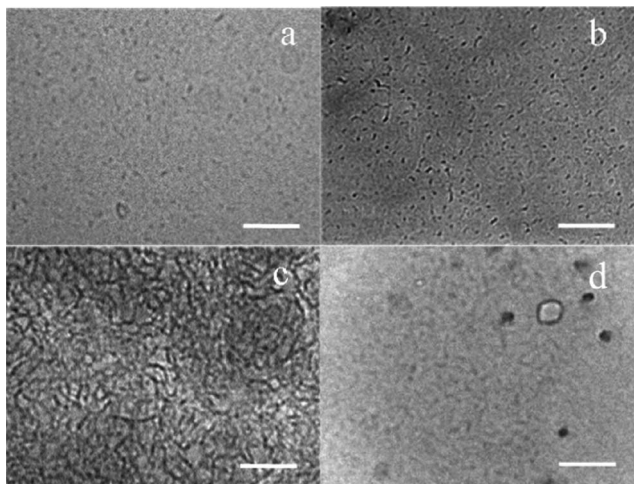


Fig. 6 The cryo-TEM images of 0.075 mol L^{-1} C10N2N at pH 9.15 (a) and 0.05 mol L^{-1} C12N2N at pH 8.48 (b) at 25°C , 0.025 mol L^{-1} C14N2N at pH = 7.55 at 40°C (c) and $0.0125 \text{ mol L}^{-1}$ C16N2N at pH 6.26 at 50°C (d). Bar represents 100 nm.

transitions when the solution pH varied from acidic to basic conditions. Simultaneously, the protonation degree of the amine groups was reduced and became unionized while continuously increasing the solution pH. As a result, the electrostatic repulsion among *CmN2N* headgroups was reduced, which has been previously confirmed by pH-dependent Zeta potential measurements in dodecyldiamines regardless of the spacer length between the two amino groups.^{12,13} Correspondingly, molecules in the aggregates can be more densely packed, and this resulted in a smaller occupied headgroup area that was confirmed by the equilibrium surface tension measurements as shown in Table 2. From the geometrical point of view, the decrease of protonation of the N-amine groups reduced the efficient headgroup area, with the occupied volume of the hydrophobic tail kept constant, and thus enlarging the effective molecular packing parameter and favoring the micelle to vesicle transition.⁵³ The effect of hydrophobic chain length *m* on the

efficient headgroup area is limited for *CmN2N* homologues at the same protonation state as mentioned in Section 3.2, while the occupied volume of the hydrophobic tail is increased significantly upon increasing *m*. Therefore, the increase of hydrophobic chain length *m* favors the micellar growth and results in the micelle to vesicle transition, shifting towards lower pH.

3.3.2 THERMALLY INDUCED MICELLE TO VESICLE TRANSITION. Interestingly, it was observed that the rodlike micelles in C10N2N, C12N2N and C14N2N can reversibly transform into vesicles upon heating or cooling, whereas C16N2N does not. The transitions were monitored by the temperature dependent SLS measurements (ESI Fig. S4[†]). For one thing, the transition pH region for C10N2N, C12N2N and C14N2N was dependent on their hydrophobic tail length, which shifted towards a lower pH value when the hydrophobic length increased. On the other hand, the transition temperature was dependent on the solution pH. Generally, a higher value of pH corresponds to a lower transition temperature for each *CmN2N*. The typical thermally induced reversibility monitored by SLS for C10N2N at pH = 9.15, C12N2N at pH = 8.48 and C14N2N at pH = 7.55 is shown in Fig. 8a. Clearly, a significant scattering intensity jump was observed above a special temperature for each sample both in heating and cooling curves. Moreover, the scattering light intensity can be recovered after a cycle, suggesting a thermally reversible micelle to vesicle transition. Hysteresis was observed after a heating and cooling cycle for each *CmN2N*, which was often observed during the thermally induced micelle to vesicle transition process by employing turbidity measurements, and may result from the structural transition dynamics.^{12,54}

Alternatively, such thermally reversible transitions were also confirmed by the temperature dependent viscosity measurements. The typical result of C12N2N at pH = 8.48 is shown in Fig. 8b, and similar results of C10N2N at pH = 9.15 and C14N2N at pH = 7.55 are shown in ESI Fig. S5.[†] It was observed that the viscosity of C12N2N was decreased upon heating, and that it recovered once the temperature went back to its initial state. Additionally, the shear thickening behavior that appeared in the

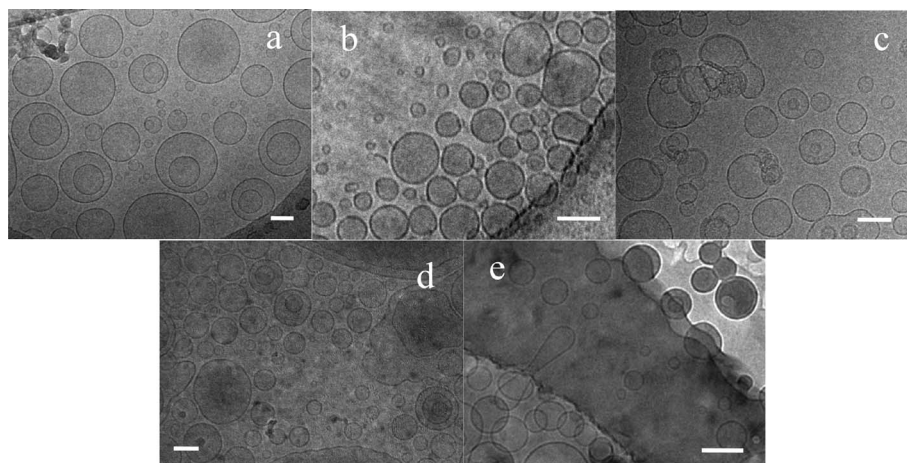


Fig. 7 The cryo-TEM images of 0.1 mol L^{-1} C8N2N at pH = 10.11 (a), 0.075 mol L^{-1} C10N2N at pH = 10.51 (b) and 0.05 mol L^{-1} C12N2N at pH = 9.80 (c) at 25°C , 0.025 mol L^{-1} C14N2N at pH = 8.83 at 40°C (d) and $0.0125 \text{ mol L}^{-1}$ C16N2N at pH = 8.28 at 50°C (e), respectively. Bar represents 100 nm.

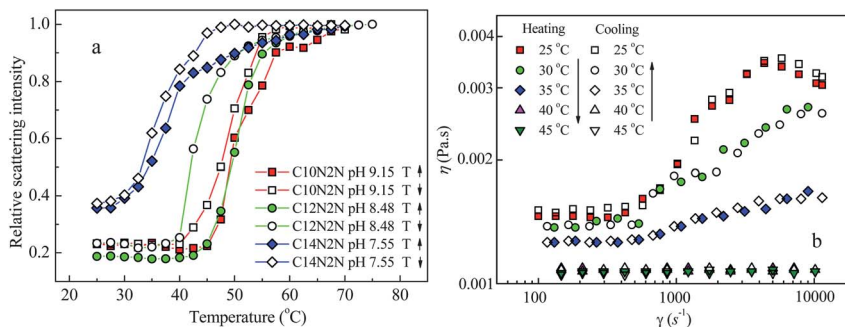


Fig. 8 (a) The scattered light intensity at $\theta = 173^\circ$ as a function of the temperature of samples containing 0.075 mol L^{-1} C10N2N, 0.05 mol L^{-1} C12N2N and 0.025 mol L^{-1} C14N2N; (b) the steady-shear rheology of 0.05 mol L^{-1} C12N2N at pH = 8.48 upon heating and cooling.

steady-shear rheology curve was weakened upon heating, and even disappeared when the temperature was higher than 40°C . However, the shear thickening behavior can also be recovered upon cooling, suggesting thermal reversibility.

Fig. 9a shows the size distribution of C10N2N at pH = 9.15, C12N2N at pH = 8.48 and C14N2N at pH = 7.55 at 60°C measured by DLS. It was observed that they all appeared to be monomodal distributions with an $R_{h,app}$ of 60, 34, and 30 nm, respectively, which were significantly different from the corresponding broad distributions of the rodlike micelles. The cryo-TEM images of these samples shown in Fig. 9b–d verified the formation of vesicles. Thus, the results of light scattering, viscosity and cryo-TEM demonstrated the thermally reversible micelle to vesicle transitions in C10N2N, C12N2N and C14N2N.

Similar thermally induced micelle to vesicle transitions have been reported previously in several systems such as nonionic surfactant,⁵⁵ ionic surfactant–cosurfactant mixed systems⁵⁶ and even catanionic surfactant systems,^{57,58} in which the thermally induced dehydration of surfactant headgroups was the major cause. Herein, C m N2N appeared to be the mixtures of HA^+ and A type surfactants in the rodlike micelles formation pH region.

Therefore, their hydrophilic headgroups contain both the ionic type ammonium and nonionic type amine, and hence C m N2N should impart some nonionic character. It has been previously demonstrated by temperature dependent ^1H NMR in *N*-dodecyl-1,3-diaminopropane that the resonances of the headgroups become broadened with a decrease in intensity upon heating,¹³ suggesting the loss of hydrogen bonding interactions between N-amine groups and water molecules. In other words, the dehydration of the hydrophilic headgroups happened at a higher temperature and resulted in their decreased hydrophilicity. Thus, the micelle to vesicle transition beyond a certain temperature of C m N2N might be due to the dehydration of the hydrophilic headgroups, which leads to the decrease in effective headgroup area and favors the formation of vesicles.

Additionally, the effective headgroup area of ionic type C m N2N is much larger than that of the nonionic one due to the electrostatic repulsion as shown in Table 2, and the increase of the $[\text{A}]/[\text{HA}^+]$ ratio should make the surfactant molecules more closely packed in the oriented molecular layers. As a result, the effective molecular packing parameter value of the system will increase and be closer to the case of vesicle formation.⁵⁸ Thus,

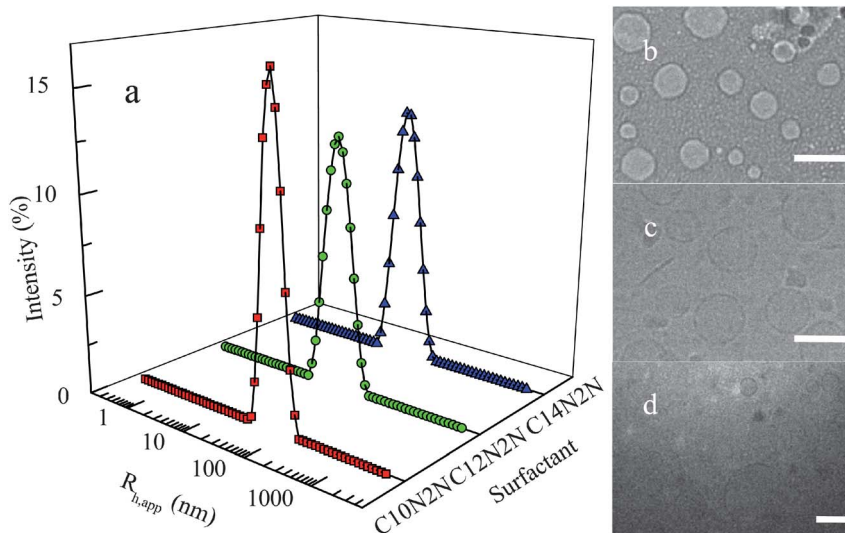


Fig. 9 (a) The apparent hydrodynamic radius $R_{h,app}$ of 0.075 mol L^{-1} C10N2N at pH = 9.15, 0.05 mol L^{-1} C12N2N at pH = 8.48 and 0.025 mol L^{-1} C14N2N at pH = 7.55 at 60°C ; the corresponding cryo-TEM images of C10N2N (b), C12N2N (c) and C14N2N (d) at 70°C , respectively. Bar represents 100 nm.

the micelle to vesicle transition can take place at a lower temperature when the solution pH is increased. Moreover, no such transition was observed for the wormlike micelle solution of C16N2N at pH = 6.26 from 25 °C even up to 80 °C (ESI Fig. S4d†), in which the light scattering intensity only increases slightly. It was noticed that wormlike micelles formed at a pH around 6.0 in C16N2N (Fig. 4a) where C16N2N appeared to be a mixture of H₂A²⁺ and HA⁺ type surfactants (ESI Fig. S1†), which was different from the HA⁺ and A type surfactant mixtures for C10N2N, C12N2N or C14N2N, where thermally induced micelle to vesicle transitions happened. Worthy of note is that the presence of A type CmN2N (*m* = 10, 12 and 14) is proved to be critical to the transition temperature (ESI Fig. S4a–c†). Though the dehydration induced cloud phenomena were observed both in ionic and nonionic surfactant systems,^{59–61} it was well known that the effect of temperature on nonionic surfactants was much stronger than on ionic ones.^{40,46} Therefore, the presented divalent H₂A²⁺ type surfactants in C16N2N might weaken the dehydration of headgroups, and hinder the micelle to vesicle transition.

4 Conclusions

In summary, we have studied the pH-dependent adsorption behaviors of CmN2N in detail, and demonstrated that the pH induced micelle to vesicle transition is a general feature due to the efficient headgroup area decrease. The length of the hydrophobic tail has little effect on the self-assembly behaviors. Moreover, thermally reversible micelle to vesicle transitions were observed in C10N2N, C12N2N and C14N2N in a certain pH region where rodlike micelles were formed, whereas not in C16N2N.

Compared with previous reports on monoalkyldiamines,^{30–36} the innovation of this work is clear. Firstly, the surface properties were studied, and the pH-dependency was also considered. Secondly, the pH-dependent self-assembly behaviors of CmN2N have been well revealed, in which the aggregate morphology is strongly related to its protonation state. Finally, the thermal reversibility of aggregates was studied for the first time. The present work provides more detailed evidence in understanding the structure–property relationship of such environmentally responsive surfactants at the molecular level. Owing to its excellent surface activity and multiple environmental sensitivity, CmN2N might find important applications in enhancing oil recovery, demulsification, nano-material synthesis, and controlled drug release. This work also indicates that bifunctional amino groups play an important role in conferring the richness in self-assembly morphologies, which might be a universal phenomenon in similar chemicals as bifunctional N-oxides of alkyldiamidoamines.^{47,48}

Acknowledgements

This work was financially supported by the National Natural Science Foundation of China (NSFC 20973129 and 21273165) and the PetroChina Innovation Foundation (2011D-5006-0205).

References

- 1 E. Chevallier, A. Mamane, H. A. Stone, C. Tribet, F. Lequeux and C. Monteux, *Soft Matter*, 2011, **7**, 7866.
- 2 A. M. Ketner, R. Kumar, T. S. Davies, P. W. Elder and S. R. Raghavan, *J. Am. Chem. Soc.*, 2007, **129**, 1553.
- 3 D. Kogelnig, A. Stojanovic, F. Kammer, P. Terzieff, M. Galanski, F. Jirsa, R. Krachler, T. Hofmann and B. K. Keppler, *Inorg. Chem. Commun.*, 2010, **13**, 1485.
- 4 P. Brown, A. Bushmelev, C. P. Butts, J. Cheng, J. Eastoe, I. Grillo, R. K. Heenan and A. M. Schmidt, *Angew. Chem., Int. Ed.*, 2012, **51**, 2414.
- 5 K. Tsuchiya, Y. Orihara, Y. Kondo, N. Yoshino, T. Ohkubo, H. Sakai and M. Abe, *J. Am. Chem. Soc.*, 2004, **126**, 12282.
- 6 A. Mohanty, T. Patra and J. Dey, *J. Phys. Chem. B*, 2007, **111**, 7155.
- 7 F. M. Menger and L. Shi, *J. Am. Chem. Soc.*, 2009, **131**, 6672.
- 8 L. Li, Y. Yang, J. F. Dong and X. F. Li, *J. Colloid Interface Sci.*, 2010, **343**, 504.
- 9 H. Kawasaki, M. Souda, S. Tanaka, N. Nemoto, G. Karlsson, M. Almgren and H. Maeda, *J. Phys. Chem. B*, 2002, **106**, 1524.
- 10 W. Wang, W. Lu and L. Jiang, *J. Phys. Chem. B*, 2008, **112**, 1409.
- 11 Z. Jiang, X. F. Li, G. F. Yang, L. Cheng, B. Cai, Y. Yang and J. F. Dong, *Langmuir*, 2012, **28**, 7174.
- 12 X. F. Li, Y. Yang, J. Eastoe and J. F. Dong, *ChemPhysChem*, 2010, **11**, 3074.
- 13 Y. Yang, J. F. Dong and X. F. Li, *J. Colloid Interface Sci.*, 2012, **380**, 83.
- 14 T. S. Davies, A. M. Ketner and S. R. Raghavan, *J. Am. Chem. Soc.*, 2006, **128**, 6669.
- 15 S. Argentiore, L. Blasi, G. Morello and G. Gigli, *J. Phys. Chem. C*, 2011, **115**, 16347.
- 16 Y. C. Liu, A. M. Le Ny, J. Schmidt, Y. Talmon, B. F. Chmelka and C. T. Lee Jr, *Langmuir*, 2009, **25**, 5713.
- 17 J. Rubio, I. Alfonso, M. I. Burguetea and S. V. Luis, *Soft Matter*, 2011, **7**, 10737.
- 18 Y. X. Liu, P. G. Jessop, M. Cunningham, C. A. Eckert and C. L. Liotta, *Science*, 2006, **313**, 958.
- 19 N. Fomina, J. Sankaranarayanan and A. Almutairi, *Adv. Drug Delivery Rev.*, 2012, **64**, 1005.
- 20 H. Y. Lee, K. R. Tiwari and S. R. Raghavan, *Soft Matter*, 2011, **7**, 3273.
- 21 S. A. Stevenson and G. J. Blanchard, *J. Phys. Chem. B*, 2006, **110**, 13005.
- 22 R. Bordes, M. Vedrenne, Y. Coppel, S. Franceschi, E. Perez and I. Rico-Lattes, *ChemPhysChem*, 2007, **8**, 2013.
- 23 P. F. Long, A. X. Song, D. Wang, R. H. Dong and J. C. Hao, *J. Phys. Chem. B*, 2011, **115**, 9070.
- 24 K. Morigaki and P. Walde, *Curr. Opin. Colloid Interface Sci.*, 2007, **12**, 75.
- 25 H. Kawasaki, R. Imahayashi, S. Tanaka, M. Almgren, G. Karlsson and H. Maeda, *J. Phys. Chem. B*, 2003, **107**, 8661.
- 26 H. Maeda, S. Tanaka, Y. Ono, M. Miyahara, H. Kawasaki, N. Nemoto and M. Almgren, *J. Phys. Chem. B*, 2006, **110**, 12451.

- 27 H. Maeda and R. Kakehashi, *Adv. Colloid Interface Sci.*, 2000, **88**, 275.
- 28 Y. H. Li, J. B. Huang, R. Zheng, M. Mao and H. L. Fu, *Chem. J. Chin. Univ.*, 2002, **23**, 1143.
- 29 X. He, B. Y. Zhu, J. B. Huang and G. X. Zhao, *J. Colloid Interface Sci.*, 1999, **220**, 338.
- 30 C. Li, X. C. Lu, X. Z. Luo and Y. Q. Liang, *Chem. Commun.*, 2001, 1440.
- 31 X. C. Lu, Z. Q. Zhang and Y. Q. Liang, *Langmuir*, 1997, **13**, 533.
- 32 C. Li, X. C. Lu and Y. Q. Liang, *Langmuir*, 2002, **18**, 575.
- 33 D. A. Jaeger, V. B. Reddy, N. Arulsamy, D. S. Bohle, D. W. Grainger and B. Berggren, *Langmuir*, 1998, **14**, 2589.
- 34 H. T. Guo, X. H. Zhou, J. F. Dong, G. Y. Zhang and X. L. Hong, *Colloids Surf., A*, 2006, **277**, 151.
- 35 X. C. Lu, Z. Q. Zhang and Y. Q. Liang, *Langmuir*, 1996, **12**, 5501.
- 36 H. Hagslaett, O. Soederman, B. Joensson and L. B. Johansson, *J. Phys. Chem.*, 1991, **95**, 1703.
- 37 S. Bhattacharya and S. K. Samanta, *J. Phys. Chem. Lett.*, 2011, **2**, 914.
- 38 R. Zana, *Adv. Colloid Interface Sci.*, 2002, **97**, 205.
- 39 J. R. Kanicky and D. O. Shah, *Langmuir*, 2003, **19**, 2034.
- 40 M. J. Rosen, *Surfactants and Interfacial Phenomena*, John Wiley & Sons, New York, 2nd edn, 1989.
- 41 F. M. Menger, L. Shi and S. A. A. Rizvi, *J. Am. Chem. Soc.*, 2009, **131**, 10380.
- 42 F. M. Menger, L. Shi and S. A. A. Rizvi, *Langmuir*, 2010, **26**, 1588.
- 43 J. Laven and G. D. With, *Langmuir*, 2011, **27**, 7958.
- 44 F. M. Menger, S. A. A. Rizvi and L. Shi, *Langmuir*, 2011, **27**, 7963.
- 45 H. B. Klevens, *J. Am. Oil Chem. Soc.*, 1953, **30**, 74.
- 46 G. X. Zhao and B. Y. Zhu, *Principles of Surfactant Action*, China Light Industry Press, Beijing, 2003.
- 47 A. Piasecki, S. Karczewski and I. Maliszewska, *J. Surfactants Deterg.*, 2007, **10**, 93.
- 48 A. Piasecki, B. Wójcik, J. Łuczyński, D. Piłakowska-Pietras, S. Witek and A. Krasowska, *J. Surfactants Deterg.*, 2009, **12**, 201.
- 49 G. Para, E. Jarek, P. Warszyński and Z. Adamczyk, *Colloids Surf., A*, 2003, **222**, 213.
- 50 G. Para, E. Jarek and P. Warszynski, *Colloids Surf., A*, 2005, **261**, 65.
- 51 R. Zana and J. Xia, *Gemini Surfactants*, Marcel Dekker Inc., New York, 2003.
- 52 J. N. Israelachvili, *Intermolecular and Surface Force*, Academic Press, New York, 2nd edn, 1991.
- 53 J. Dehmoune, J. P. Decruppe, O. Greffier, H. Xu and P. Lindner, *Langmuir*, 2009, **25**, 7271.
- 54 P. R. Majhi and A. Blume, *J. Phys. Chem. B*, 2002, **106**, 10753.
- 55 G. Wanka, H. Hoffmann and W. Ulbricht, *Colloid Polym. Sci.*, 1990, **268**, 101.
- 56 H. Hoffmann, K. Horbaschek and F. Witte, *J. Colloid Interface Sci.*, 2001, **235**, 33.
- 57 H. Q. Yin, Z. K. Zhou, J. B. Huang, R. Zheng and Y. Y. Zhang, *Angew. Chem., Int. Ed.*, 2003, **42**, 2188.
- 58 H. Q. Yin, J. B. Huang, Y. Y. Lin, Y. Y. Zhang, S. C. Qiu and J. P. Ye, *J. Phys. Chem. B*, 2005, **109**, 4104.
- 59 K. S. Sharma, S. R. Patil and A. K. Rakshit, *Colloids Surf., A*, 2003, **219**, 67.
- 60 S. R. Raghavan, H. Edlund and E. W. Kaler, *Langmuir*, 2002, **18**, 1056.
- 61 P. Mukherjee, S. K. Padhana, S. Dashb, S. Patelc and B. K. Mishra, *Adv. Colloid Interface Sci.*, 2011, **162**, 57.